THE ASTROPHYSICAL JOURNAL, 218:269–285, 1977 November 15

CHARGE COMPOSITION AND ENERGY SPECTRA OF COSMIC-RAY NUCLEI AT ENERGIES ABOVE 5 GeV PER NUCLEON*†

JOHN H. CALDWELL
Enrico Fermi Institute and Department of Physics, University of Chicago
Received 1977 March 7; accepted 1977 May 11

ABSTRACT

A scintillation-Cerenkov counter telescope, with three gas Cerenkov counters for energy determination between 5 and 90 GeV per nucleon, has been exposed for a net total of 4.5 m^2 sr hr in two balloon flights in 1974. The measurement yields the chemical composition and energy spectra of cosmic-ray nuclei in the charge range $5 \leq Z \leq 28$. The differential spectral indices of oxygen and of the iron group are measured to be 2.67 ± 0.04 and 2.50 ± 0.08 above 5.4 GeV per nucleon, respectively. The results are interpreted in the context of the "leaky-box" model of cosmic-ray confinement and propagation. The cosmic-ray leakage path length λ is found to have the energy dependence $\lambda \propto E_{\rm tot}^{-0.59 \pm 0.09}$. After this energy-dependent propagation has been incorporated into the model, it is found that the measurements are consistent with an energy-independent source composition for the cosmic rays.

Subject headings: cosmic rays: abundances — cosmic rays: general

I. INTRODUCTION

A powerful method in the study of the origin and propagation of the cosmic radiation is the measurement of the charge composition and energy spectra of cosmic-ray nuclei. The nuclei that are detected at the Earth are composed not only of primary particles, which originated in the cosmic-ray sources, but also of secondary nuclei which were produced in nuclear interactions of source nuclei with the interstellar gas during their propagation. From the relative abundances of the primary particles, one can infer the nuclear composition at the source. On the basis of spectroscopic measurements and nucleosynthesis calculations, some nuclear species which appear as secondaries are believed to be completely absent at the cosmic-ray sources. A measurement of the abundances of such species can yield a value for the amount of matter traversed by the progenitors of the secondary nuclei.

Until recently, the experimental data were consistent with an energy independence of the relative abundances of cosmic-ray nuclei. Models of cosmic-ray production and propagation were thus constructed with energy-independent source composition and energy-independent propagation in the Galaxy. Measurements reported in the last few years have conclusively shown that the relative abundances of cosmic-ray nuclei are different above about 5 GeV per nucleon than they are below a few GeV per nucleon (Juliusson, Meyer, and Müller 1972; Smith *et al.* 1973; Balasubrahmanyan and Ormes 1973; Webber *et al.* 1973; Juliusson 1974). The most pronounced change observed is the decrease at high energies of the relative abundance of secondary nuclei when compared with primary particles. This has been interpreted as indicating that high-energy particles traverse less matter than those at low energy, and thus produce fewer secondary nuclei. An unambiguous explanation for the origin of this energy-dependent path length, however, has yet to be advanced. While this is primarily due to large uncertainties in the astrophysical parameters that enter into any cosmic-ray model, disparities in the observations are also a problem. In addition to the intrinsic difficulties involved in making differential energy measurements above a few GeV per nucleon, the spectrum of the cosmic radiation is so steep that, even with the large instruments and long exposure times now possible during balloon flights, large statistical uncertainties remain in the data.

Variations in the energy spectra of source nuclei have also been reported, leading to speculation that more than one discrete source, or type of source, of cosmic rays is needed to explain the observations. There still exist, however, significant differences between experiments on such important abundance ratios as those of carbon to oxygen, and oxygen to iron; and thus one should be cautious of the presence of systematic effects. One difficulty results from the fact that each experiment covers a limited energy range, and therefore sometimes results from several groups have been combined to establish the existence of an energy dependence (e.g., Lund 1975).

An important step toward identifying the energy dependence of the chemical abundance of cosmic rays at high energies was accomplished by the work of Juliusson (1974). His instrument used a plastic Cerenkov counter to measure energies between 0.5 and

* This work was supported in part by the National Aeronautics and Space Administration under grant NGL 14-001-005.

† Submitted to the Department of Physics, University of Chicago, in partial fulfillment of the requirements for the Ph.D. degree.

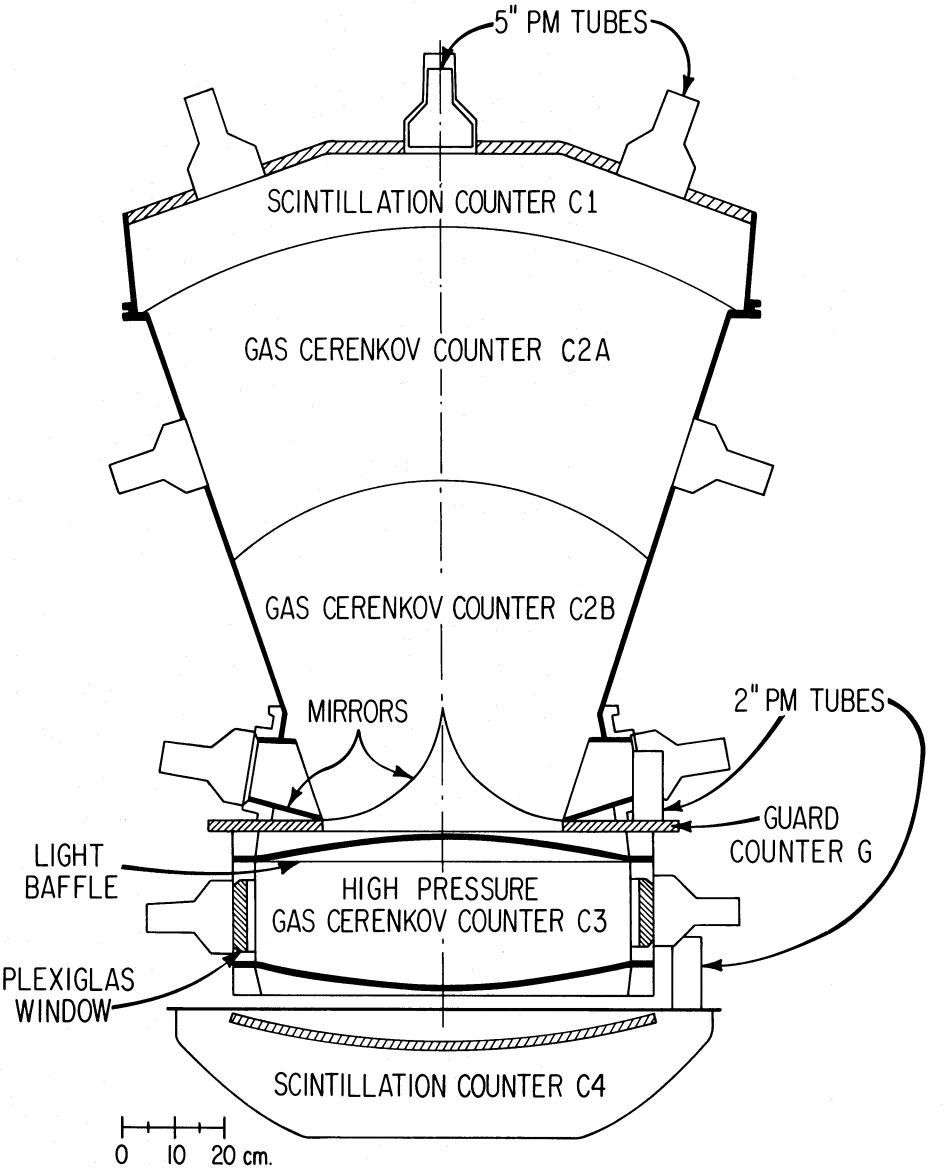

FIG. 1.—A schematic cross section of the instrument

4 GeV per nucleon, and two gas Cerenkov counters for energy determination above 20 GeV per nucleon. We felt that a significant improvement to the observational data could be made if the instrument used by Juliusson were modified to allow energy measurement between 5 and 20 GeV per nucleon, and if such an instrument were exposed for an additional time to accumulate more data above 20 GeV per nucleon. These goals have been accomplished with the inclusion of a high-pressure gas Cerenkov counter and through two successful balloon flights in 1974. Preliminary results have been reported by Caldwell and Meyer (1975). In this paper we present a high-resolution study of the chemical composition of cosmic-ray nuclei, over the energy range 5 to 90 GeV per nucleon.

II. INSTRUMENT AND BALLOON FLIGHTS

The detector used in this experiment is a scintillation-Cerenkov counter telescope, which is shown schematically in Figure 1. The earlier version of this instrument, referred to above, is described by Juliusson (1974). The two scintillation counters, C1 and C4, are the charge-determining elements. Both scintillators are made from Pilot Y and are 11 mm thick. They are situated in light-diffusion chambers to maximize uniformity of response over the detector surface. Another technique used to improve the charge resolution of the instrument was to shape C1 and C4 to reduce path-length variations in these counters. The C1 scintillator is segmented into six parts, each of

which is perpendicular to the line connecting the center of that part to the center of the hole in the guard counter. The bottom scintillator, C4, was heat formed into a portion of a spherical shell with radius of curvature calculated to reduce the path-length distribution to its theoretical minimum (Perkins *et al.* 1969; Sullivan 1971). We calculate the relative standard deviation, σ/mean, of the path-length distribution in either C1 or C4 to be approximately 2%.

The energy measurements made by this instrument are accomplished by three gas Cerenkov counters with different indices of refraction. Multiple Cerenkov counters were used for two reasons. First, the Cerenkov effect is strongly dependent on the energy of the particle only over a limited range of energy, as can be seen in the relation

$$L \propto (1 - P_0^2/P^2) . \quad (1)$$

Here L is the Cerenkov light yield and P is the momentum per nucleon of the incident particle in atomic mass units. The momentum per nucleon of a particle is a function only of its velocity, as can be seen by the equality $P = \beta\gamma$, where β is the ratio of the velocity to the speed of light, and γ is the Lorentz factor. The threshold momentum per nucleon of the radiator, below which there will be no Cerenkov light, is denoted by P_0, and this quantity is equal to $1/(n^2 - 1)^{1/2}$, where n is the index of refraction of the Cerenkov radiator. It is easily verified from equation (1) that excellent energy resolution can be obtained from a Cerenkov counter only from the threshold momentum to a value of about 3 times threshold. Thus to cover a large range of energy, as is desired in this experiment, more than one Cerenkov counter with appropriately chosen indices of refraction are necessary.

There is a second advantage of having multiple Cerenkov counters in an instrument. In gas Cerenkov counters, with their low index of refraction, the number of photons produced by a relativistic particle is small. Thus it is possible that a nucleus with energy below the Cerenkov threshold can produce a spurious signal of the same magnitude as the Cerenkov signal, for instance, by the passage of a δ-ray through the window of a photomultiplier tube. One must be able to reject such background events, and an excellent method of accomplishing this is to use several counters. It is then possible to require that consistent signals be present in the various Cerenkov counters.

The high-pressure gas Cerenkov counter C3 is the major new component of the instrument. It is a light-diffusion chamber that is filled with ethylene gas at 18.6 atm at 20° C. The threshold kinetic energy of this detector is 5 GeV per nucleon. The cylindrical wall of the pressure chamber is made of 2 inch (5 cm) thick 6061-O aluminum, through which 10 portholes have been drilled. Plexiglas windows are lodged in the portholes to retain the pressure, and allow protection of the windows of the photomultiplier tubes that view the interior of the chamber. The top and bottom of the pressure vessel are fashioned of 0.25 inch (0.63 cm) 2024-T3 aluminum. A very thin light baffle in the upper part of the chamber reduces the path-length variation to about 3%. The mean path length through the counter is 24 cm, along which a singly charged highly relativistic particle produces a signal corresponding to 12 photoelectrons. The other two gas Cerenkov counters C2A and C2B operate at a pressure of one atmosphere. C2A is a light-diffusion chamber, filled with isobutane gas, which has a Cerenkov threshold of 17 GeV per nucleon. C2B, on the other hand, is a focusing gas Cerenkov counter which contained carbon dioxide during the first flight and Freon-12 for the second. The thresholds of these two gases are 30 and 19 GeV per nucleon, respectively.

The instrument also contains an annular guard scintillator. This counter is used to define the coincidence requirement, $C1 \cdot \overline{G} \cdot C4$, which has a geometric factor of 910 cm^2 sr. The guard counter is also used to help in the rejection of nonnuclear background. It, and all other counters in this instrument, are pulse-height analyzed.

The instrument was flown twice from Palestine, Texas, in 1974 fall. The first flight remained at a ceiling altitude of 4 g cm^{-2} of residual atmosphere for 12 hours. The second flight lasted over 42 hours, although during the second night the balloon descended from 4 to about 11 g cm^{-2}. The total net exposure factor for the flights amounted to 4.5 m^2 sr hr.

III. DATA ANALYSIS

a) Event-Selection Criteria and Correction Factors

In order for an event to be accepted for further analysis, it must fulfill two main selection criteria. These criteria are designed to select nuclei that pass through the instrument without interacting and without being accompanied by background particles. The first criterion rejects events that produce a large signal in the guard counter. The guard counter cannot be in strict anticoincidence, however, since δ-rays produced by a nucleus can cause a signal in the guard, even if the primary particle passed through the hole in the guard counter. The selection criterion used is that the signal in the guard be less than 8% of that signal which would have occurred had the primary nucleus passed through the guard scintillator. The criterion will also aid in rejecting nonnuclear background such as atmospheric side showers. The charge-dependent effects of this criterion have been investigated. At maximum, the criterion eliminates approximately 2% of the noninteracting nuclei of a given charge. Selection-correction factors are applied to remove any bias in the data imposed by event selection.

The second selection criterion is consistency in the pulse heights from the scintillators C1 and C4. In order to select noninteracting nuclei, it is required that the ratio of the signals produced in the two identical scintillators C1 and C4 vary from unity by less than a factor that is equal to 20% at beryllium and decreases linearly as a function of atomic number to 8% at iron. A charge-dependent criterion is applied to ensure that interacting particles are effectively eliminated. The

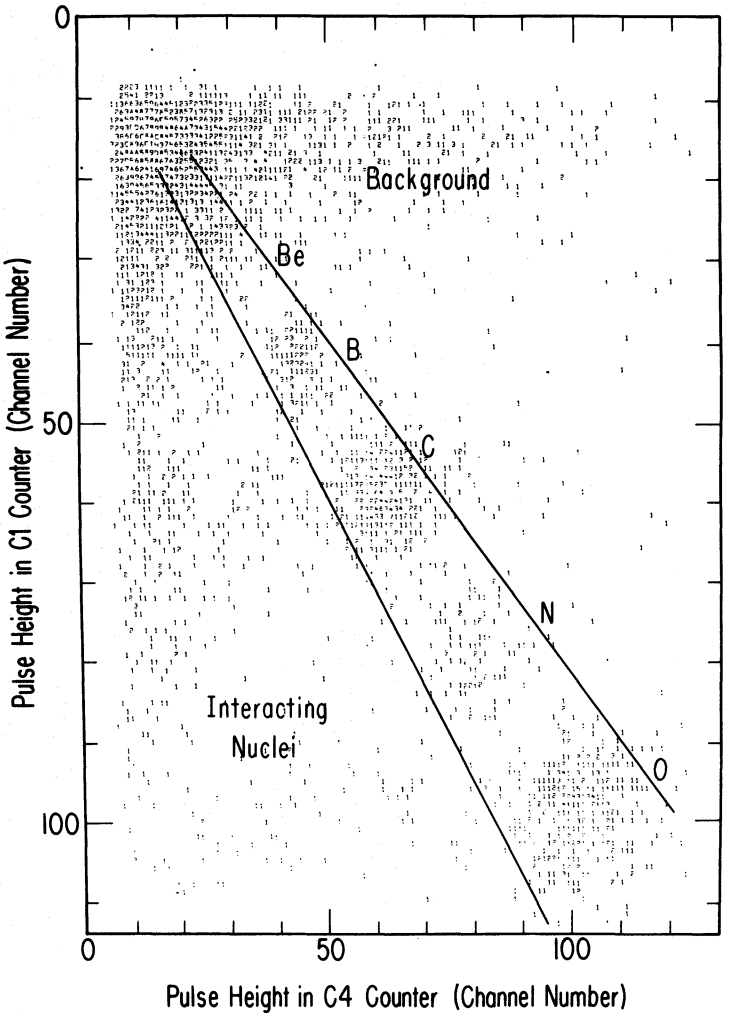

FIG. 2.—Scatter plot of pulse height in C1 counter versus pulse height in C4 counter for events with energy above 5.4 GeV per nucleon that satisfy the guard counter selection criterion. These data were obtained in 4 hours during the first balloon flight. The scintillator agreement selection criterion accepts only those events that lie between the two lines.

selection will again reject some nuclei improperly, and thus appropriate selection-correction factors have to be applied.

Application of the scintillator agreement criterion is illustrated in Figure 2. In this, a scatter plot of the pulse heights in the two scintillators C1 and C4 is displayed. The events included are from 4 hours of the first flight, have energies above 5.4 GeV per nucleon as determined by the C3 gas Cerenkov counter, and satisfy the guard counter criterion. The scintillator agreement criterion rejects events that lie outside the two lines. This excludes the vast majority of background events and interacting nuclei. Although there is good charge separation for the charges above beryllium in this figure, there is a concentration of background events for the lowest charges. The origin of this background is uncertain, but it is probably due to the simultaneous passage of multiple particles. From the number of such events, we can infer that they are induced by cosmic-ray protons, which are about 100 times more abundant than all nuclei with charge greater than 2. Because of this problem, we have chosen to exclude lithium and beryllium completely from our analysis and to consider boron subject to a background correction.

b) Charge Determination

The charge of a nucleus is determined from the average of the square roots of the signals in the two scintillators C1 and C4. The scintillator signals were corrected for saturation, drift, and finite channel-width effects and small nonlinearities in the pulse-height analyzers. A histogram of nuclei with energy greater than 5.4 GeV per nucleon that satisfy the guard counter and scintillator agreement selection criteria is shown in Figure 3. The standard deviation of the charge measurement at carbon is 0.18 charge units.

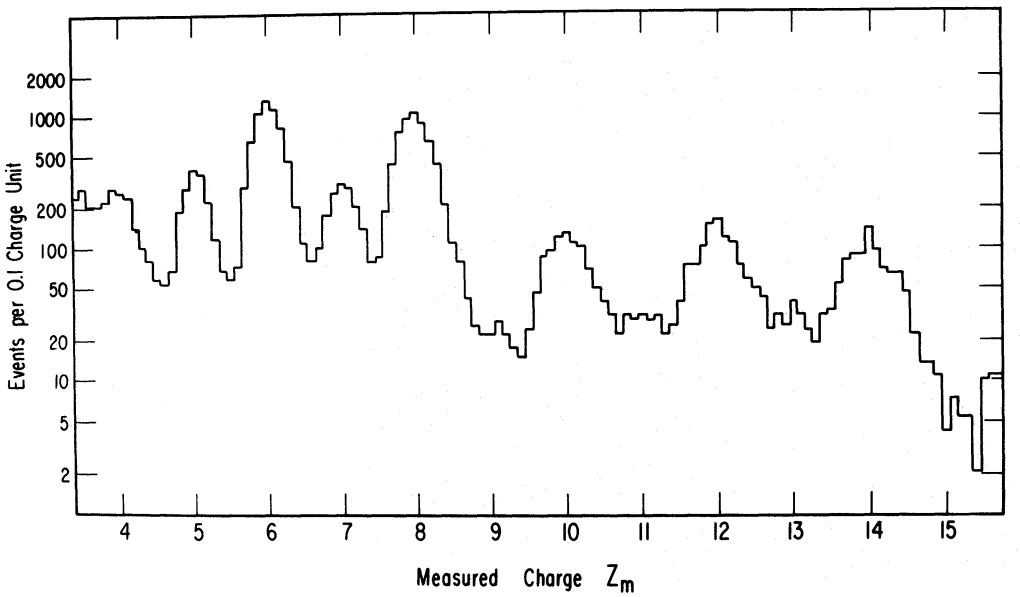

FIG. 3.—A histogram of the measured charge of nuclei above 5.4 GeV per nucleon that satisfy the selection criteria. Note the logarithmic scale of the abscissa.

One straightforward method of determining the number of nuclei of charge Z from a charge histogram such as Figure 3 would be to count all nuclei with measured charge $Z_m = Z \pm 0.5$. This number would need to be corrected for the overlapping of one charge into the region assigned to its neighboring charges. This charge-overlap correction would depend on the charge resolution of the instrument and the relative abundances of the elements. The value 0.5 for the charge interval half-width is arbitrary, and, as discussed by Juliusson (1974), smaller charge-overlap corrections can result if different values are chosen. We have adopted the following criteria for charge intervals: $Z_m = Z_0 \pm 0.375$ for the odd integer charges, $Z_m = Z_e \pm 0.625$ for the even integer charges except iron, and $Z_m = 26 \pm 1.375$ for iron, where Z_0 and Z_e are the appropriate integer charge numbers. Iron is allowed a wide interval because the charge resolution in this region is such (0.35 charge units) that it would not be meaningful to assign separate charge bins to the rare elements manganese and cobalt.

c) *Energy Determination*

For the purposes of this paper, we divide the energy region measured by the instrument into three parts. Low-energy nuclei will correspond to particles above the geomagnetic cutoff that yet have insufficient energy to trigger the high-pressure gas Cerenkov counter. This region thus contains energies from 1.6 to 5.4 GeV per nucleon, although the lower limit is approximate because of the drift of the instrument in geomagnetic latitude during a balloon flight. Medium-energy data will refer to those events that do produce Cerenkov light in the high-pressure gas counter, and are below the Cerenkov threshold of the C2A gas counter. Thus this energy region corresponds to 5.4 to 17 GeV per nucleon. Nuclei with energy greater than the C2A gas Cerenkov counter threshold, 17 GeV per nucleon, are denoted as high energy. As discussed in § II, the Cerenkov counters are used to make the energy measurements in this experiment. For the medium-energy region, the parameter used to determine the energy was the signal in the high-pressure Cerenkov counter C3 divided by the square of the charge of the nucleus. The pulse-height distributions produced by oxygen nuclei in the C3 gas Cerenkov counter and by iron nuclei in the C2A gas Cerenkov counter are presented in Figure 4. The events included in these histograms have satisfied both the guard counter and scintillator agreement selection criteria. In order to extract an energy spectrum from such plots, one must (1) determine the location of the Cerenkov threshold in the presence of residual scintillation in the gas; (2) determine the $\beta = 1$ point of the distribution; and (3) calculate the deconvolution corrections that must be applied to remove the effect of finite detector resolution. The $\beta = 1$ point is the signal that a particle traveling with the speed of light would produce, if the detector had infinite pulse-height resolution. The energy-pulse-height correspondence from such calculations are shown in Figure 4 by arrows.

In the high-energy region of analysis, the signal from the C2A Cerenkov counter divided by the square of the charge is the parameter utilized to determine the energy of the particle. For an event to be accepted as being of high energy, however, it must also satisfy two additional requirements. The event must have high energy as measured in C3, and it must have a consistent pulse height in the C2B Cerenkov counter.

The Cerenkov thresholds in C3 and C2A are easily found, since the scintillation component is small, amounting to only 4% of the $\beta = 1$ signal in the high-pressure counter and 8% in the isobutane detector.

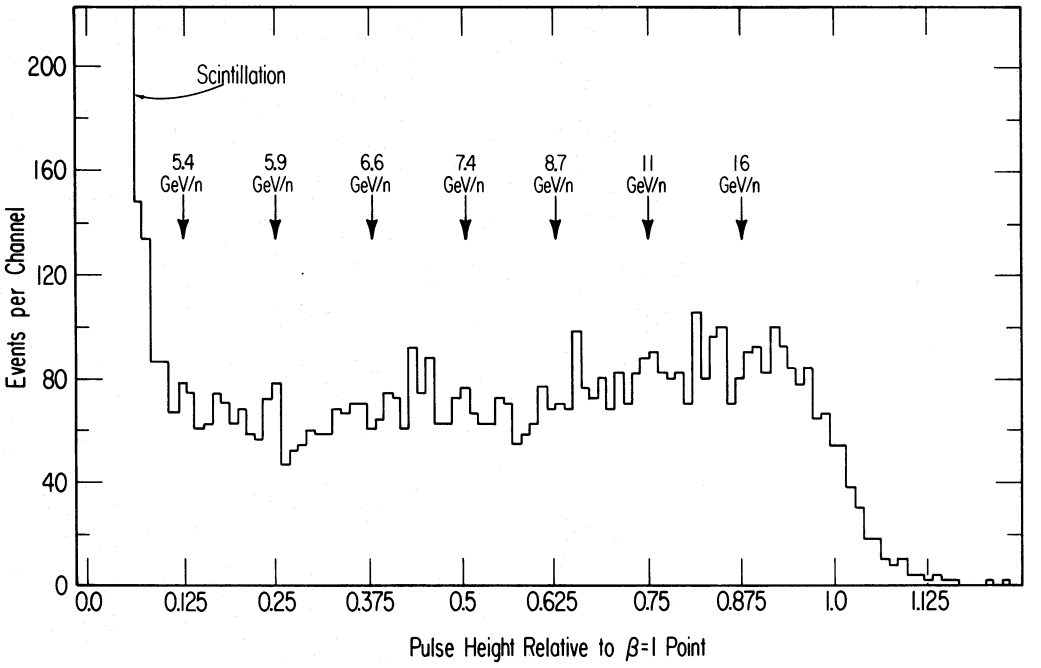

FIG. 4a

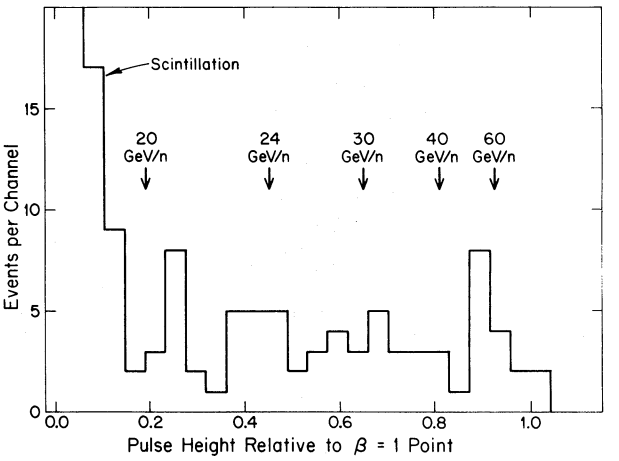

FIG. 4b

FIG. 4.—(*a*) Pulse-height distribution in the C3 high-pressure gas Cerenkov counter for oxygen nuclei. (*b*) Pulse-height distribution in the C2A gas Cerenkov counter for iron nuclei. The energies corresponding to the pulse heights are indicated by arrows. The $\beta = 1$ point is the signal that a particle traveling with the speed of light would produce if the detector had infinite resolution.

The $\beta = 1$ point in the C3 gas Cerenkov counter can be found quite accurately by selecting events that produce a large signal in the C2A Cerenkov detector. Finding the $\beta = 1$ point in the C2A counter, however, must be done from the data themselves. This introduces the possibility of systematic error in the energy measurement in the high-energy region. The deconvolution correction factors are calculated by the statistical deconvolution technique described by Juliusson (1974).

Stated briefly, this method is as follows. If a Cerenkov counter had infinite pulse-height resolution, a simple inversion of equation (1) would supply the desired relation between energy and pulse height. Real Cerenkov detectors have finite resolution, of course, attributable to such sources as fluctuations in the number of photoelectrons produced in the photomultiplier tubes and the path-length variations in the detector. We have written a computer code to simulate, in a Monte Carlo sense, the operation of the Cerenkov counters C3 and C2A. A power law ($\propto E_{\rm tot}{}^{-2.7}$) for the cosmic-ray spectrum is assumed. Using randomly chosen energies from this distribution, and folding the appropriate instrumental response function into equation (1), we produce a simulated Cerenkov pulse-height distribution. Since we do know the connection between

the actual energy and the measured pulse height for the simulated events, deconvolution corrections can be developed for the actual distribution measured by the instrument. If the resulting energy spectrum is significantly different from the assumed, the procedure is repeated until a self-consistent spectrum is obtained.

As discussed by Lezniak (1976), the production of Cerenkov light by δ-rays, although important in a Lucite Cerenkov radiator, is negligible in gas Cerenkov counters, such as those used in this experiment. We therefore do not further consider this effect.

d) Interaction and Atmospheric Corrections

Two additional corrections are necessary to obtain the nuclear composition at the top of the atmosphere. Cosmic-ray nuclei can undergo charge-altering interactions both in the instrument and in the overlying atmosphere. Different locations of the interaction will lead to different responses of the instrument to the interacting particle. It is possible that the fragments from the interaction will pass through the counters in such a manner as to violate one of the selection criteria. In this case it is necessary to correct the observed abundance for the loss of a nucleus. The interaction can also, however, go undetected by the instrument, and thus a nucleus will be recorded, but it will be one with a different charge than the original incident particle.

The first of the two possible responses will be corrected for by the interaction correction. For the event to be rejected by the scintillator selection criterion, we believe that the interaction must take place in one of the following; the lower half of the C1 scintillator (0.57 g cm^{-2}), the matter between C1 and C4 (6.5 g cm^{-2}), or the upper half of the C4 scintillator (0.57 g cm^{-2}). To calculate the magnitude of this correction, use has been made of the total nucleus-nucleus reaction cross section of Meyer, Cassé, and Westergaard (1975). Since this formula is based on recent accelerator data rather than older emulsion work, we believe it to be quite accurate.

If an interaction takes place in the residual atmosphere, the matter in the instrument above C1 (1.8 g cm^{-2}), or the upper half of the C1 scintillator (0.57 g cm^{-2}), it is believed that the instrument will record a nucleus with an altered charge. This change in composition is removed by the atmospheric correction, which unfortunately is neither easily nor accurately calculable. We have constructed a model of the propagation of high-energy cosmic rays in the atmosphere. The major input necessary to this calculation is the nucleus-nucleus (*N-N*) fragmentation cross sections, of which only an extremely small number have been determined experimentally. Fortunately, because of the observed factorization of *N-N* cross sections (Heckman *et al.* 1972), *N-N* cross sections are relatable to proton-nucleus (*p-N*) cross sections by a scale factor dependent only on the target. Using then the *p-N* cross sections derived from the semiempirical formulae of Silberberg and Tsao (1973*a*, *b*), supplemented wherever possible by experimental results (e.g., Lindstrom *et al.* 1975), and the scale factors of Silberberg, Tsao, and Shapiro (1976), we have calculated a complete set of *N-N* fragmentation cross sections. The propagation through the atmosphere was accomplished by numerically integrating the equation of transport using a δ-function (slab) path-length distribution for 232 nuclides between ^{64}Ni and ^{6}Li. This calculation includes all isotopes as stable within that range with decay half-lives greater than 10^{-6} s. Since we consider only high-energy cosmic rays, we can neglect the effect of ionization energy loss and treat the fragmentation cross sections as energy-independent. The abundances at the top of the atmosphere were chosen so that the calculated abundances at the atmospheric depth of the instrument were consistent with our measured values at 8 GeV per nucleon. The resulting abundances as a function of depth were summed over the isotopes for a given element; the corrections are given in Table 1.

TABLE 1

ATMOSPHERIC CORRECTIONS FOR THE RELATIVE ABUNDANCES OF COSMIC RAYS

Z		This Experiment	Juliusson (1974)
5.....	Boron	-9.7	-15
6.....	Carbon	-11	-16
7.....	Nitrogen	-6.2	-8
8.....	Oxygen	...	...
9.....	Fluorine	-1.6	-2
10.....	Neon	-0.7	0
11.....	Sodium	-1.4	-1
12.....	Magnesium	+0.5	+1
13.....	Aluminum	-0.6	0
14.....	Silicon	+1.6	+2
15-24....	VH Group*	-2.8	0
25-28....	Iron Group	+2.8	+4

NOTE.-- Correction to be added to measured abundance relative to oxygen (oxygen = 1000) to correct for 1.0 g cm^{-2} of overlaying atmosphere.

*Very heavy nuclei.

IV. RESULTS

a) Relative Abundances

Only data from the first flight were used for the low-energy region. In the second flight, C3 was added to the coincidence requirement to reduce a loss of events because of dead time in the analyzers. The average energy for the low-energy interval is 2.5 GeV per nucleon. Events with a C3 signal less than 12.5% of the $\beta = 1$ point were divided into charge intervals as described in § III*b*. The raw numbers, corrections, and abundances relative to oxygen for the low-energy data are presented in Table 2. A background correction was made for boron, amounting to the removal of 6% of the events in that charge interval. We estimate that the background correction is known to a factor of 25%. The corrected number is shown in parentheses in the table. For the abundant elements boron to

1977ApJ...218..269C

TABLE 2

NUMBER OF LOW ENERGY NUCLEI, (<E> = 2.5 GeV PER NUCLEON), SATISFYING SELECTION CRITERIA, CORRECTIONS, AND RELATIVE ABUNDANCES

Element	Raw Number	Charge Overlap Correction (M)*	Selection Correction (M)	Interaction Correction (M)	Relative Abundance at top of Instrument (R > 4.7 GV and E < 5.4 GeV/nucleon)	Atmospheric Correction (A)*	Rigidity-to-Energy Conversion Factor (M)	Relative Abundance at top of Atmosphere (<E> = 2.5 GeV/n)
Boron.....	1364 (1282)	1.03	1.11	0.958	0.454 ± 0.017	-0.063	0.90	0.35 ± 0.02
Carbon.....	3770	0.99	1.05	0.969	1.226 ± 0.030	-0.072	1.00	1.15 ± 0.03
Nitrogen...	1065	1.05	1.02	0.987	0.361 ± 0.013	-0.040	0.95	0.30 ± 0.01
Oxygen.....	3136	0.99	1.00	1.000	1.000 ± 0.025	0.0	1.00	1.00 ± 0.02
Fluorine...	99	1.04	0.99	1.020	0.034 ± 0.003	-0.010	0.91	0.02 ± 0.01
Neon.....	563	0.98	0.99	1.030	0.182 ± 0.008	-0.005	0.96	0.17 ± 0.01
Sodium.....	167	1.08	0.98	1.047	0.060 ± 0.005	-0.009	0.93	0.05 ± 0.01
Magnesium..	596	0.98	0.97	1.056	0.192 ± 0.009	+0.003	0.97	0.19 ± 0.01
Aluminum...	138	1.10	0.97	1.072	0.051 ± 0.004	-0.004	0.94	0.04 ± 0.01
Silicon....	443	0.99	0.97	1.079	0.149 ± 0.008	+0.010	0.99	0.16 ± 0.01
VH Group+..	467	1.00	1.02	1.146	0.176 ± 0.008	-0.018	0.94	0.15 ± 0.01
Iron Group.	265	1.00	1.18	1.235	0.124 ± 0.008	+0.018	0.88	0.13 ± 0.01

*Type of correction: M = multiplicative, A = additive.
+Very heavy nuclei.

TABLE 3

NUMBER OF MEDIUM ENERGY NUCLEI SATISFYING SELECTION CRITERIA, AND SELECTION CORRECTIONS

Median Energy	5.6 GeV/n	6.2 GeV/n	7.0 GeV/n	8.0 GeV/n	9.6 GeV/n	13. GeV/n	
Bin Edges, GeV/n	5.4 – 5.9	5.9 – 6.6	6.6 – 7.4	7.4 – 8.7	8.7 – 11.	11. – 16.	Selection Correction
Boron	248 (233)	225 (212)	245 (230)	219 (206)	229 (215)	224 (211)	1.13
Carbon	790	765	838	782	839	953	1.05
Nitrogen	234	220	207	212	239	197	1.02
Oxygen	736	650	776	714	832	954	1.00
Fluorine	29	23	24	28	33	35	0.99
Neon	119	126	117	116	137	127	0.98
Sodium	34	20	25	28	33	44	0.97
Magnesium	112	122	131	133	150	167	0.97
Aluminum	18	22	29	24	31	39	0.97
Silicon	83	108	83	114	122	155	0.97
VH Group*	66	65	77	82	94	111	1.01
Iron	38	39	39	36	61	64	1.14
Nickel	4	1	1	3	2	2	1.23

*Very heavy nuclei, $15 \leq Z \leq 24$.

silicon, charge overlap significantly affects the abundance ratios. The charge-overlap correction was determined from an unfolding procedure

$$N(Z) = \sum_{Z'} P_{ZZ'}{}^{-1} \times N_m(Z') . \qquad (2)$$

Here $N(Z)$ is the true number of nuclei with charge Z, $N_m(Z')$ is the measured number of nuclei with charge Z', and $P_{ZZ'}$ is the probability that a nucleus of charge Z' has a measured charge Z. Selection-correction factors are then applied to account for the imperfection of the two main selection criteria. Interaction and atmospheric corrections are applied as described in § III*d*. The final correction converts the low-energy data from an abundance measurement above a rigidity threshold to one above an energy threshold. This is done to make the low-energy data directly comparable with the medium- and high-energy results. In order to calculate this conversion factor, one needs the isotopic composition of each element in the cosmic rays at several GeV per nucleon. We have used experimental results wherever possible (Dwyer and Meyer 1975, 1977), but for the majority of the elements we must rely on a propagation model. For propagation in the Galaxy, we used the "leaky-box" model, which has an exponential distribution of vacuum particle path lengths (see Ginzburg and Ptuskin 1976 for a recent description). The propagation calculation included as stable the 78 isotopes between ^{64}Ni and ^{6}Li with decay half-lives greater than 10^7 years. The elemental source abundances were those of Shapiro, Silberberg, and Tsao (1975), with the isotopic abundance ratios of solar system material (Cameron 1973). The fragmentation cross sections were obtained similarly to those in § III*d*, but scale factors appropriate for interstellar propagation were utilized. The calculational technique used was the matrix method of Cowsik and Wilson (1973). The source abundances were propagated through a mean value of 6.5 g cm^{-2} of interstellar matter (90% *p*, 10% He, by number). From the results of this calculation, the mean mass of each element in the arriving cosmic rays was determined, allowing the desired conversion factors to be calculated.

Events with a signal in the high-pressure gas Cerenkov counter C3 such that $0.125 \leq C3/Z^2 \leq 0.875$ are considered medium-energy data. The lower restriction prevents low-energy nuclei that produce scintillation light in C3 from contaminating the medium-energy region. The upper limit is applied to make the medium-energy events a set distinct from the high-energy data. The events that satisfy the C3 signal restriction and the selection criteria are divided into charge intervals and energy bins, and the resulting raw numbers are shown in Table 3. The same small background correction as in the low-energy data is applied to the boron events, and the corrected number is shown in parentheses in the table. No charge-overlap corrections are applied, since the magnitude of these corrections is much less than the statistical uncertainty of the numbers. The selection corrections for the medium-energy data are shown in the last column of the table. It was found that the scintillator resolution became slightly worse with increasing energy (consistent with increasing Vavilov fluctuations), and thus different selection-correction factors need to be used for this energy region. The same interaction correction, however, is appropriate for all energies. When these corrections are applied, we can calculate the relative abundances of the medium-energy nuclei between 5.4 and 16 GeV per nucleon, which are displayed in Table 4.

The analysis of the high-energy data is similar to that in the medium-energy region. Besides the two main selection criteria, we require that a high-energy event possess a signal in the high-pressure counter $0.875 \leq C3/Z^2 \leq 1.30$. It was found that this criterion is so effective in rejecting background that no correction is necessary for boron, and use of the velocity information from the C2B gas Cerenkov counter yields no further improvement in the quality of the data. The raw numbers, divided into charge and energy intervals, are displayed in Table 5. These numbers must be multiplied with the interaction correction from Table 2 and the selection-correction factors for

1977ApJ...218..269C

TABLE 4

RELATIVE ABUNDANCES FOR MEDIUM ENERGY COSMIC RAY NUCLEI AT 7.1 g/cm^2 IN THE ATMOSPHERE

Z	Element	Kinetic Energy						Atmospheric Correction
		5.6 GeV/n	6.2 GeV/n	7.0 GeV/n	8.0 GeV/n	9.6 GeV/n	13 GeV/n	
5.....	Boron	0.343 ± 0.027	0.352 ± 0.029	0.321 ± 0.025	0.312 ± 0.026	0.280 ± 0.022	0.239 ± 0.019	-0.069
6.....	Carbon	1.092 ± 0.056	1.197 ± 0.064	1.099 ± 0.055	1.114 ± 0.058	1.026 ± 0.050	1.016 ± 0.047	-0.078
7.....	Nitrogen	0.320 ± 0.024	0.341 ± 0.027	0.269 ± 0.021	0.299 ± 0.023	0.283 ± 0.021	0.208 ± 0.016	-0.044
8.....	Oxygen	1.000 ± 0.052	1.000 ± 0.055	1.000 ± 0.051	1.000 ± 0.053	1.000 ± 0.049	1.000 ± 0.096	0.0
9.....	Fluorine	0.040 ± 0.007	0.036 ± 0.008	0.031 ± 0.006	0.040 ± 0.008	0.040 ± 0.007	0.037 ± 0.006	-0.011
10.....	Neon	0.163 ± 0.016	0.196 ± 0.019	0.152 ± 0.015	0.164 ± 0.016	0.166 ± 0.015	0.134 ± 0.013	-0.005
11.....	Sodium	0.047 ± 0.008	0.031 ± 0.007	0.033 ± 0.007	0.040 ± 0.008	0.040 ± 0.007	0.047 ± 0.007	-0.010
12.....	Magnesium	0.156 ± 0.016	0.192 ± 0.019	0.173 ± 0.016	0.191 ± 0.018	0.185 ± 0.016	0.179 ± 0.015	+0.004
13.....	Aluminum	0.025 ± 0.006	0.035 ± 0.008	0.039 ± 0.007	0.035 ± 0.007	0.039 ± 0.007	0.043 ± 0.007	-0.004
14.....	Silicon	0.118 ± 0.014	0.174 ± 0.018	0.112 ± 0.013	0.167 ± 0.017	0.153 ± 0.015	0.170 ± 0.015	+0.011
15-24.....	VH Group*	0.104 ± 0.013	0.114 ± 0.015	0.114 ± 0.014	0.131 ± 0.015	0.129 ± 0.014	0.132 ± 0.013	-0.020
25-28.....	Iron Group	0.081 ± 0.013	0.087 ± 0.014	0.073 ± 0.012	0.077 ± 0.013	0.107 ± 0.014	0.097 ± 0.012	+0.020

*Very heavy nuclei.

TABLE 5

NUMBER OF HIGH ENERGY NUCLEI SATISFYING SELECTION CRITERIA, AND SELECTION CORRECTIONS

Median Energy	22 GeV/n	27 GeV/n	34 GeV/n	47 GeV/n	90 GeV/n	
Bin Edges, GeV/n	20	24	30	40	60	Selection Correction
Boron.....	52	34	25	11	4	1.19
Carbon.....	226	195	132	131	58	1.10
Nitrogen.....	55	38	33	21	13	1.03
Oxygen.....	244	174	143	123	81	1.00
Fluorine.....	5	9	6	2	0	0.98
Neon.....	26	23	19	16	12	0.97
Sodium.....	6	3	4	1	3	0.95
Magnesium.....	46	33	22	26	24	0.94
Aluminum.....	10	8	7	5	3	0.94
Silicon.....	35	35	29	17	9	0.94
VH Group*.....	27	21	16	14	8	0.98
Iron.....	25	16	12	12	7	1.11
Nickel.....	2	1	0	0	0	1.20

*Very heavy nuclei, $15 \leq Z \leq 24$.

high-energy nuclei which are given in the last column of Table 5. One final correction is necessary before the relative abundances can be calculated. The light yield in the C2A gas Cerenkov counter is so small, namely, about one photoelectron per singly charged highly relativistic particle, that the deconvolution corrections mentioned in § III*c* need to be applied to the three highest-energy bins. These corrections are displayed in Figure 5. The relative abundances for the high-energy data are given in Table 6.

Using the data from Tables 2, 4, and 6, we have plotted in Figure 6 the relative abundance ratios B/(C + O) and $(15 \leq Z \leq 24)/(25 \leq Z \leq 28)$ as a function of energy from 2.5 to 90 GeV per nucleon. Both these ratios are of nuclei that are predominantly secondary in origin to those that are presumed to be mostly primary. In this figure we have also shown the source value of each ratio, as calculated by Shapiro, Silberberg and Tsao (1975). The ratios shown in Figure 6 display the characteristic decrease at high energy in the abundance of a secondary species relative to its progenitors. This phenomenon must be caused by a decrease in the amount of matter traversed in the interstellar medium by the primary nuclei. It is obvious, from the closeness of our values of these ratios at high energy to their source abundances, that the interstellar cosmic-ray path length above 50 GeV per nucleon is very short.

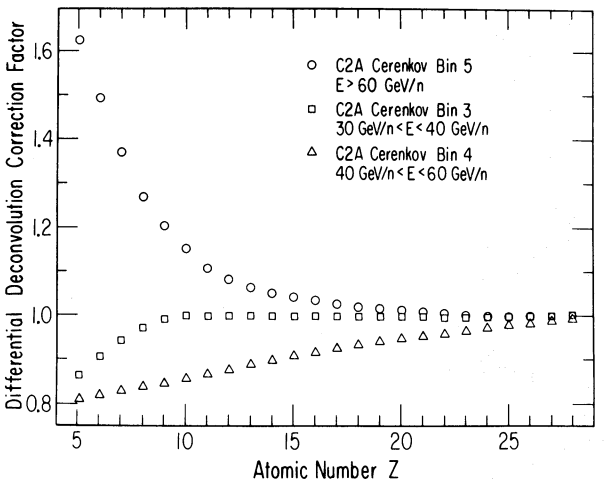

FIG. 5.—Differential deconvolution correction factors as a function of atomic number Z for the C2A gas Cerenkov counter. The correction is multiplicative, is equal to unity for the two C2A Cerenkov bins lowest in energy, and is calculated by the technique of Juliusson (1974).

In Figure 7, we show two primary/primary ratios. In both cases the group of elements that is of smaller average mass number is placed in the numerator of the ratio. The source ratios in this figure have the same meaning as in Figure 6. A slight decrease with energy is expected in a light primary/heavy primary ratio, because of the reduction in interstellar path length at high energy. Only if a relative abundance ratio falls significantly below its source value can it be stated unequivocally that no propagation model alone can explain such a variation. The first ratio shown in Figure 7 is that of (C + O)/(Ne + Mg + Si). While this ratio is relatively energy-independent, it does show a small decrease with increasing energy to a value consistent with the source ratio. The second ratio displayed in this figure shows a suggestion of structure in the energy spectrum of the iron group nuclei. The ratio $(\text{Ne} + \text{Mg} + \text{Si})/(25 \leq Z \leq 28)$ seems to have, superposed on a general decrease with increasing energy, a possible enhancement at about 6 GeV per nucleon and is flat above 20 GeV per nucleon. These effects may well be due to statistical fluctuations, however, and are mentioned here only because of an intriguingly similar shape of the iron group/(C + O) ratio that was reported by Orth, Buffington, and Smoot (1975). The iron group elements are generally defined as $25 \leq Z \leq 28$.

b) Absolute Flux and Energy Spectra

The additional factors necessary to convert the raw number of observed oxygen nuclei to absolute flux are the absolute values of the interaction, selection, atmospheric, and deconvolution (if appropriate) corrections

TABLE 6

RELATIVE ABUNDANCES OF HIGH ENERGY COSMIC RAY NUCLEI AT 7.1 g/cm^2 IN THE ATMOSPHERE

Z	Element	Kinetic Energy 22 GeV/n	27 GeV/n	34 GeV/n	47.0 GeV/n	90.0 GeV/n
5.....	Boron	0.24 ± 0.04	0.22 ± 0.04	0.18 ± 0.04	0.10 ± 0.03	0.07 ± 0.04
6.....	Carbon	0.99 ± 0.09	1.19 ± 0.12	0.91 ± 0.11	1.11 ± 0.14	0.90 ± 0.16
7.....	Nitrogen	0.23 ± 0.03	0.22 ± 0.04	0.23 ± 0.04	0.17 ± 0.04	0.18 ± 0.05
8.....	Oxygen	1.00 ± 0.09	1.00 ± 0.11	1.00 ± 0.12	1.00 ± 0.13	1.00 ± 0.16
9.....	Fluorine	0.02 ± 0.01	0.05 ± 0.02	0.04 ± 0.02	0.02 ± 0.01	0.00 ± 0.01
10.....	Neon	0.11 ± 0.02	0.13 ± 0.03	0.14 ± 0.03	0.14 ± 0.04	0.13 ± 0.04
11.....	Sodium	0.02 ± 0.01	0.02 ± 0.01	0.03 ± 0.02	0.01 ± 0.01	0.03 ± 0.02
12.....	Magnesium	0.19 ± 0.03	0.19 ± 0.04	0.16 ± 0.04	0.22 ± 0.05	0.25 ± 0.06
13.....	Aluminum	0.04 ± 0.01	0.05 ± 0.02	0.05 ± 0.02	0.04 ± 0.02	0.03 ± 0.02
14.....	Silicon	0.15 ± 0.03	0.20 ± 0.04	0.22 ± 0.04	0.15 ± 0.04	0.09 ± 0.03
15-24.....	VH Group*	0.12 ± 0.02	0.13 ± 0.03	0.13 ± 0.04	0.14 ± 0.04	0.09 ± 0.03
25-28.....	Iron Group	0.15 ± 0.03	0.13 ± 0.03	0.12 ± 0.04	0.16 ± 0.05	0.09 ± 0.09

*Very heavy nuclei.

for that element and the exposure factor for the flights. These numbers are presented in Table 7, and the resulting absolute differential fluxes for the low- and medium-energy data are plotted in Figure 8*a*. We have chosen to first extract integral flux measurements from the high-energy data. To do this, an integral deconvolution correction is needed, and its magnitude is given in Table 7. The integral flux values for the high-energy data are plotted in Figure 8*b*, along with those of Juliusson (1974). The spectrum from our experiment is slightly steeper, the best power-law fit in total energy in the least-squares sense yielding an integral spectral index of 1.81 ± 0.11, while Juliusson (1974) obtained a value for the spectral index of 1.59 ± 0.13. The figure demonstrates, however, that the difference is entirely in the two points lowest in energy. In Juliusson *et al.* (1975), the authors reject the point lowest in energy of Juliusson (1974) and give the point next higher in energy only half-weight.

The best power-law fit to the integral spectrum of

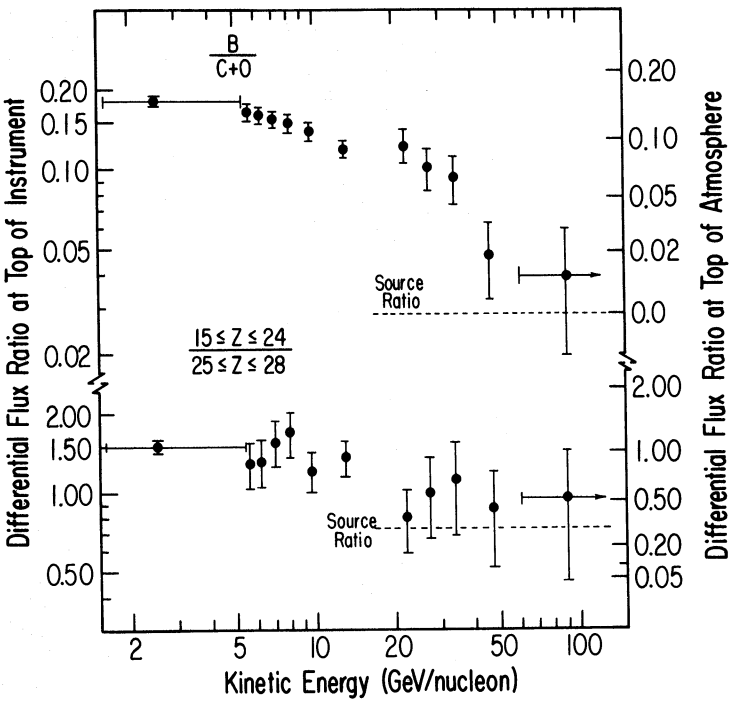

FIG. 6.—Two secondary/primary ratios measured in this experiment as a function of energy. Primary nuclei are presumed to have been present in the cosmic-ray source, while secondary nuclei are considered to have been created in nuclear interactions of the primary nuclei with the interstellar medium during their propagation from the cosmic-ray source. The dashed lines are the source ratios, taken from the calculation of Shapiro, Silberberg, and Tsao (1975).

TABLE 7

FACTORS NECESSARY TO CALCULATE THE ABSOLUTE FLUX OF OXYGEN

	Interaction Correction	Selection Correction	Atmospheric Correction	Integral Deconvolution Correction	Exposure Factor (m^2 sr hr)
Low Energy Data	1.32	1.05	1.21	not applicable	0.96
Medium Energy Data	1.32	1.08	1.24	1.00	4.50
High Energy Data					
a) Energy > 60 GeV/nucleon bin	1.32	1.13	1.24	1.49	4.50
b) Other C2A bins	1.32	1.13	1.24	1.00	4.50

oxygen for the high-energy data is then differentiated to yield differential fluxes, and these points are plotted in Figure 8*a*. The uncertainties in these points reflect both the statistical uncertainty in the number of nuclei measured in each differential energy bin and the possible systematic uncertainty which arises in the correspondence of the Cerenkov pulse height with energy. A power-law fit in total energy to both the medium- and high-energy differential flux measurements yields the differential spectral index for oxygen of 2.67 ± 0.04 over the energy range 5.4 to 90 GeV per nucleon, and the line in Figure 8*a* represents this fit. The point at 2.5 GeV per nucleon is not included in this fit because of the uncertain nature of the penumbra of the geomagnetic field and also the effect of solar modulation, which flattens the cosmic-ray spectrum at these low energies.

To calculate the spectral indices of the other elements, a best power-law fit was made to the abundances relative to oxygen for the combined medium- and high-energy data, which had been corrected to the top of the atmosphere. These spectral index differences were then applied to the measured spectral index of oxygen. The results of this calculation are shown in Table 8.

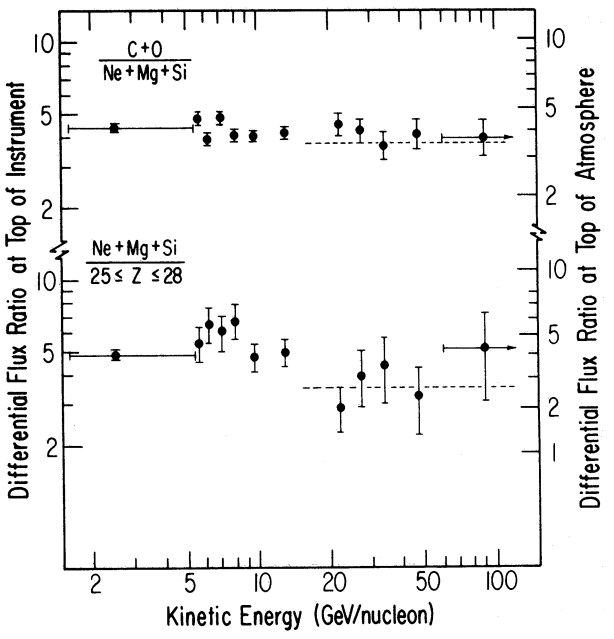

FIG. 7.—Two primary/primary ratios measured in this experiment as a function of energy. Primary nuclei are presumed to have been present in the cosmic-ray source. Dashed lines have the same meaning as in Fig. 6.

V. DISCUSSION AND CONCLUSIONS

a) The Cosmic-Ray Leakage Path Length above 2.5 GeV per Nucleon

We now consider the energy dependence of the leakage path length more quantitatively. This quantity is

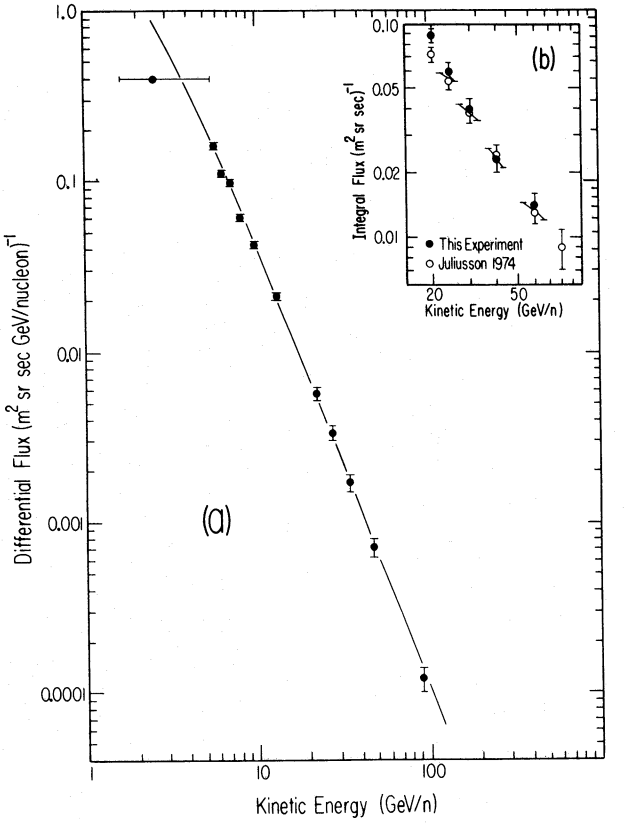

FIG. 8.—(*a*) The measured differential energy spectrum of oxygen as a function of energy. The line represents a power-law fit in total energy of the form $n(E) \propto E_{tot}^{-2.67}$. (*b*) The integral energy spectrum of oxygen above 20 GeV per nucleon, with the results of this experiment compared with those of Juliusson (1974).

TABLE 8

SPECTRAL INDICES FOR COSMIC RAYS ABOVE 5.4 GeV PER NUCLEON

Z	Element	γ*
5.....	Boron	3.35 ± 0.10
6.....	Carbon	2.76 ± 0.06
7.....	Nitrogen	3.07 ± 0.10
8.....	Oxygen	2.67 ± 0.04
9.....	Fluorine	3.01 ± 0.21
10.....	Neon	2.88 ± 0.08
11.....	Sodium	3.14 ± 0.25
12.....	Magnesium	2.60 ± 0.06
13.....	Aluminum	2.52 ± 0.10
14.....	Silicon	2.63 ± 0.11
15-24....	VH Group+	2.64 ± 0.07
25-28....	Iron Group	2.50 ± 0.08

*Spectra have been fitted to a power law in total energy, $n(E) \propto E^{-\gamma}$. Only statistical errors are shown. A systematic error of ± 0.10 should be included for each element.

+Very heavy nuclei.

determined by relating the observed energy dependence of the relative abundance of boron to oxygen with the results of the propagation model discussed in § IV*a* for a variety of mean path lengths. Since boron is assumed to be completely secondary, the amount of matter traversal that the model requires to reproduce the measured B/O relative abundance at a given energy yields the mean value of the amount of interstellar material through which the cosmic rays have propagated at that energy. The results of this calculation are shown in Figure 9, where we have grouped some data points to increase the statistical accuracy of an individual measurement. A least-squares fit to a power law in total energy yields the relation for the path length λ, $\lambda \propto E_{\rm tot}^{-0.59 \pm 0.09}$.

It was noted by Audouze and Cesarsky (1973) that if the energy dependence of the leakage path length were much steeper than $E_{\rm tot}^{-0.6}$, there would be difficulties in explaining the observed isotropy of the cosmic rays and the steepening in the cosmic-ray spectrum at about 10^6 GeV per nucleon. Our value is within this restriction and is also consistent with the determination of Juliusson *et al.* (1975). Using the data of Juliusson (1974), Smith *et al.* (1973), and Webber (1972), Juliusson *et al.* (1975) arrived at -0.49 ± 0.05 for the spectral index of the energy dependence of the path length. It should be noted that only uncertainties in the abundance measurement contribute to the error bars in Figure 9; propagation errors are not included. We do not believe, however, that the systematic error in the semiempirical cross-section formulae can significantly affect our result, since 80% of the yield of boron is now calculated from cross sections that have been measured (O'Dell *et al.* 1975).

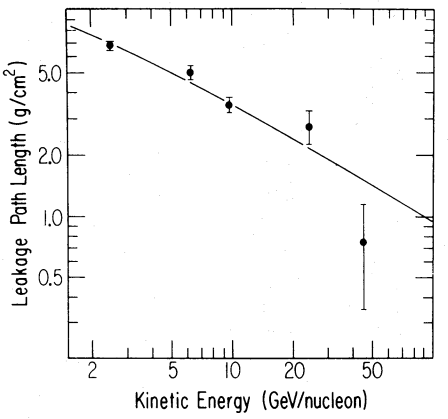

FIG. 9.—The energy dependence of the cosmic-ray leakage path length, λ, as a function of energy, as determined from the observed energy dependence of the boron/oxygen ratio. The line is a least-squares fit to the data points of the form $\lambda \propto E_{\rm tot}^{-0.59}$.

b) The Energy Dependence of the Cosmic-Ray Source Composition

The energy-dependent leakage path length derived in the last section is now incorporated into our propagation model. The assumption of energy-independent source composition is retained to test its validity. The propagation model is used to calculate the energy dependence of the elemental abundances relative to oxygen, and these predictions are compared with our measurements. We find no significant disparities that would force us to reject the notion of energy-independent source composition for any of the relative abundance measurements reported in Tables 2, 4, and 6. Claims for energy-dependent source composition in at least four elemental ratios have been made (see references below). In Figures 10 and 11 we present our data and propagation model predictions for these relative abundances as well as a compilation of recent measurements. To obviate the possibility of introducing systematic error by the use of differing atmospheric corrections, we have applied the atmospheric corrections given in Table 1 to all data shown in these two figures. The results of Juliusson *et al.* (1975) have been edited, as described in § IV*b*.

The strongest argument for the existence of energy-dependent source composition has been made in the case of carbon/oxygen (Juliusson and Meyer 1973; Juliusson 1974; and Juliusson *et al.* 1975). Our results for C/O, shown in Figure 10*a*, do not exhibit as large a decrease at high energy as did these authors. Consider also the results of Smith *et al.* (1973), which are consistent with the carbon/oxygen ratio being constant with energy. Before the important and simple assumption of similar source energy spectra for all elements can be abandoned, we believe that a more compelling discrepancy between model and data must be present. The need for more precise data, especially above 30 GeV per nucleon, is manifest. In Figure 10*b*, the ratio of carbon to silicon is plotted. Lund (1975) stated that the observed variation in this relative abundance between 0.5 and 4.0 GeV per nucleon varied by

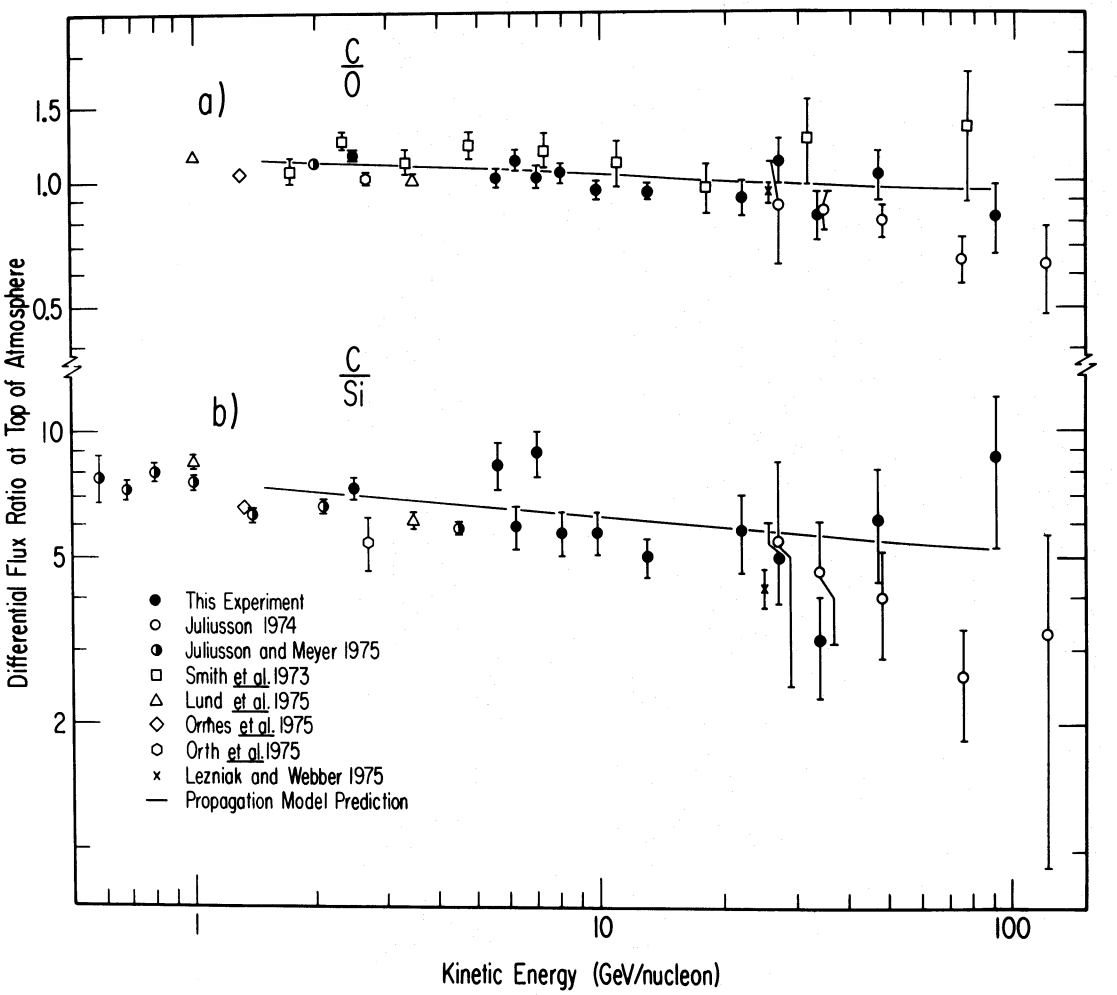

FIG. 10.—A comparison of experimental results with the predictions (*solid line*) of a cosmic-ray propagation model that contains energy-dependent leakage path length but energy-independent source composition for the two relative abundances carbon/oxygen and carbon/silicon.

a factor of 3 more than could be explained by propagation effects alone. While our data cover energies that are too high to confirm or refute Lund's conjecture, it is apparent from the data above 1.5 GeV per nucleon, shown in the figure, that the measurement and propagation model seem to be consistent. It should be noted here that there is no renormalization for each element in the propagation model. That our measurements and the propagation predictions agree for the elemental ratios other than boron to oxygen represents confirmation for the calculated source abundances of Shapiro, Silberberg, and Tsao (1975).

Juliusson *et al.* (1975) reported that the nitrogen/oxygen source abundance changed with energy. This is a very difficult determination, since nitrogen is mostly secondary (N/C at the source is 0.07 ± 0.02, according to Dwyer and Meyer 1975). Juliusson *et al.* do state that the effect is small and thus could be due to statistics. We feel that the results in Figure 11*a* demonstrate that the observed variation in the N/O ratio is well explained by an energy-independent source abundance and an energy-dependent leakage path length. The relative abundance of oxygen to the iron group has been a subject of interest for a number of years. Balasubrahmanyan and Ormes (1973) reported that the difference in spectral indices between carbon and oxygen compared with the iron group was $\Delta\gamma = 0.56 \pm 0.15$. They stated that this difference was too large to be explained only by propagation effects. Their results are not plotted in Figure 11*b* because they do not report O/iron group data separately. As pointed out by Juliusson (1975), the iron spectrum measured by Balasubrahmanyan and Ormes (1973) agrees essentially with the results of Juliusson (1974), which are plotted in the figure. Juliusson measured a difference in spectral index between oxygen and the iron group to be 0.4 ± 0.2. The results of Balasubrahmanyan and Ormes (1973) are hampered by poor

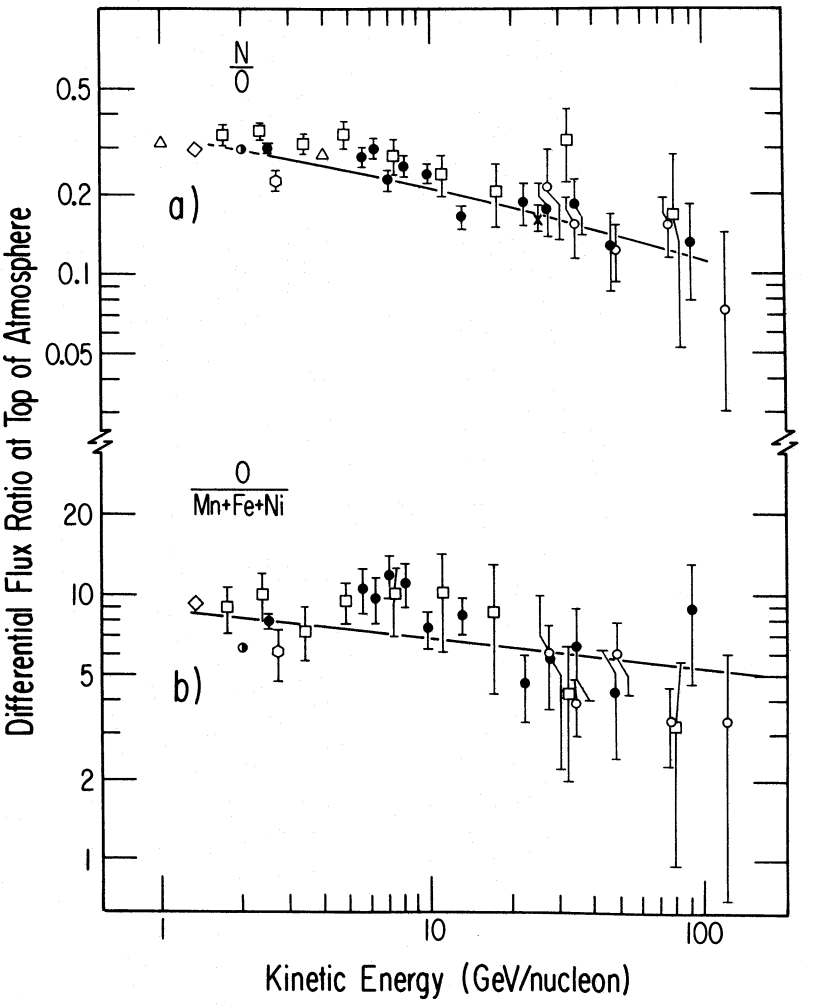

FIG. 11.—A comparison of experimental results with the predictions (*solid line*) of a cosmic-ray propagation model that contains energy-dependent leakage path length but energy-independent source composition for the two relative abundances nitrogen/oxygen and oxygen/iron group. Symbols for data refer to same authors as in Fig. 10.

statistical significance. Their spectral index difference, using only data above 8 GeV per nucleon, is $\Delta\gamma = 0.38 \pm 0.30$ (Ramaty, Balasubrahmanyan, and Ormes 1973). In agreement with Juliusson *et al.* (1975), we believe that the data and the propagation model predictions are consistent. We again note, however, the cluster of data points between 4 and 8 GeV per nucleon that are above the propagation model prediction. We feel that it would be of great interest for a future experiment to resolve the question of the existence of this effect.

c) *Implications for Cosmic-Ray Models*

The results of this experiment on the relative abundances of cosmic-ray nuclei in the energy range 5 to 90 GeV per nucleon are compatible with a "leaky-box" propagation model which has an energy-dependent leakage path length and energy-independent source composition. Thus we feel that any model that incorporates more than one cosmic-ray particle population to produce energy-dependent source composition is unnecessary within the accuracy of present observations.

The energy dependence of the cosmic-ray leakage path length $\lambda(E)$ is now well determined. Both the results of Juliusson *et al.* (1975) and those of this experiment are consistent with $\lambda(E) \propto E_{\rm tot}^{-0.5}$. Several cosmic-ray models have been created with approximately this dependence, such as the "nested leaky-box" model of Cowsik and Wilson (1973), in which cosmic rays escape from the source regions in an energy-dependent manner, but undergo energy-independent propagation in the rest of the Galaxy. This model can produce the correct form for $\lambda(E)$ by postulating a reasonable size distribution of magnetic irregularities in the source regions. It is an advantage of the model that the observed spectral indices of primary nuclei are the same as those at the source. Hence the model does not require additional power for the cosmic-ray

sources because of faster leakage from the entire confinement volume.

The author wishes to express his sincere gratitude to his faculty sponsor, Professor Peter Meyer, for his support and assistance throughout the course of this work. He would like to thank Dr. Einar Juliusson for his work on the original version of the instrument, and for many valuable suggestions concerning this project. He is also grateful to Dr. Robert Dwyer for useful discussions. The electronics engineers for this project were Gary Kelderhouse and William Hollis. Mechanical design and construction of the instrument were performed by Wayne Johnson and Anthony Kittler. Some data-analysis programming was done by Linda Glennie, Nancy Beck, Leigh Littleton, and Dr. Paul Evenson. The balloon flights were conducted by the staff of the National Scientific Balloon Facility of the National Center for Atmospheric Research.

REFERENCES

Audouze, J., and Cesarsky, C. J. 1973, *Nature Phys. Sci.*, **241**, 98.
Balasubrahmanyan, V. K., and Ormes, J. F. 1973, *Ap. J.*, **186**, 109.
Caldwell, J., and Meyer, P. 1975, *14th Internat. Cosmic-Ray Conf.* (Munich), **1**, 273.
Cameron, A. G. W. 1973, *Space Sci. Rev.*, **15**, 121.
Cowsik, R., and Wilson, L. W. 1973, *13th Internat. Cosmic-Ray Conf.* (Denver), **1**, 500.
Dwyer, R., and Meyer, P. 1975, *Phys. Rev. Letters*, **35**, 601.
———. 1977, *Ap. J.*, **216**, 635.
Ginzburg, V. L., and Ptuskin, V. S. 1976, *Rev. Mod. Phys.*, **48**, 161.
Heckman, H. H., Greiner, D. E., Lindstrom, P. J., and Bieser, F. S. 1972, *Phys. Rev. Letters*, **28**, 926.
Juliusson, E. 1974, *Ap. J.*, **191**, 331.
———. 1975, *14th Internat. Cosmic-Ray Conf.* (Munich), **8**, 2689.
Juliusson, E., and Meyer, P. 1973, *Ap. Letters*, **14**, 153.
———. 1975*a*, *14th Internat. Cosmic-Ray Conf.* (Munich), **1**, 256.
———. 1975*b*, private communication.
Juliusson, E., Cesarsky, C. J., Meneguzzi, M., and Cassé, M. 1975, *14th Internat. Cosmic-Ray Conf.* (Munich), **2**, 653.
Juliusson, E., Meyer, P., and Müller, D. 1972, *Phys. Rev. Letters*, **28**, 926.
Lezniak, J. A. 1976, *Nucl. Instr. Meth.*, **136**, 299.
Lezniak, J. A., and Webber, W. R. 1975, *14th Internat. Cosmic-Ray Conf.* (Munich), **12**, 4107.
Lindstrom, P. J., Greiner, D. E., Heckman, H. H., Cork, B., and Bieser, F. S. 1975, preprint.
Lund, N. 1975, *14th Internat. Cosmic-Ray Conf.* (Munich), **11**, 3746.
Lund, N., Lundgaard Rasmussen, I., Peters, B., and Westergaard, N. J. 1975, *14th Internat. Cosmic-Ray Conf.* (Munich), **1**, 257.
Meyer, J. P., Cassé, M., and Westergaard, N. 1975, *14th Internat. Cosmic-Ray Conf.* (Munich), **12**, 4144.
O'Dell, F. W., Shapiro, M. M., Silberberg, R., and Tsao, C. H. 1975, *14th Internat. Cosmic-Ray Conf.* (Munich), **2**, 526.
Ormes, J. F., Fisher, A., Hagen, F., Maehl, R., and Arens, J. F. 1975, *14th Internat. Cosmic-Ray Conf.* (Munich), **1**, 245.
Orth, C. D., Buffington, A., and Smoot, G. F. 1975, *14th Internat. Cosmic-Ray Conf.* (Munich), **1**, 280.
Perkins, M. A., Kristoff, J. J., Mason, G. M., and Sullivan, J. D. 1969, *Nucl. Instr. Meth.*, **68**, 149.
Ramaty, R., Balasubrahmanyan, V. K., and Ormes, J. F. 1973, *Science*, **180**, 731.
Shapiro, M. M., Silberberg, R., and Tsao, C. H. 1975, *14th Internat. Cosmic-Ray Conf.* (Munich), **2**, 532.
Silberberg, R., and Tsao, C. H. 1973*a*, *Ap. J. Suppl.*, **25**, 315 and 335.
———. 1973*b*, *Ap. J. Suppl.*, **25**, 335.
Silberberg, R., Tsao, C. H., and Shapiro, M. M. 1976, in *Spallation Nuclear Reactions and Their Applications*, ed. B. S. P. Shen and M. Merker (Dordrecht: Reidel), p. 49.
Smith, L. H., Buffington, A., Smoot, G. F., Alvarez, L. W., and Wahlig, M. A. 1973, *Ap. J.*, **180**, 987.
Sullivan, J. D. 1971, *Nucl. Instr. Meth.*, **95**, 5.
Webber, W. R. 1972, preprint.
Webber, W. R., Lezniak, J. A., Kish, J. C., and Damle, S. V. 1973, *Nature Phys. Sci.*, **241**, 96.

JOHN H. CALDWELL: Gulf Science and Technology Company, Geophysical Sciences Department, Pittsburgh, PA 15230